EML 4905 Senior Design Project

A SENIOR THESIS

PREPARED IN PARTIAL FULFILLMENT OF THE

REQUIREMENT FOR THE

DEGREE OF BACHELOR OF SCIENCE

IN MECHANICAL ENGINEERING

Design, Analysis and Multi-Objective Constrained Optimization of Multi-Winglets

Sohail Reddy
Shanae Powell
Abraham Neiss

Faculty Advisor: Dr. George S. Dulikravich

This report is written in partial fulfillment of the requirements in EML 4806. The contents represent the opinion of the authors and not the Department of

Mechanical and Materials Engineering.

ETHICS STATEMENT AND SIGNATURES

This project is submitted as a B.S. thesis is solely the work of the following team. Sohail Reddy , Shanae Powell and Abraham Neiss. Any works quoted has been stated as such, and proper credit is given to the original authors. This pertains to all the engineer drawings and all other analysis as well.

_____	_____	_____
Sohail Reddy	Shanae Powell	Abraham Neiss
Team Member	Team Member	Team Member

Dr. George Dulikravich

Faculty Advisor

Table of Contents

Abstract 7

Chapter I: Introduction 7

1.2 Problem statement 7

1.2 Motivation 8

1.3 Literature Review 9

1.3.1 Theories of Lift and Drag 9

1.3.2 The Kutta-Zhukowsky Condition 10

1.3.3 Helmholtz Laws 11

1.3.4 Stall Characteristics of Airfoils 13

1.3.5 The Finite Wing Theory 14

1.3.6 Flow Field Around Finite Wings 14

1.4 Methods of Induced Drag Reduction and Retardation of Vortex Formation 15

1.4.1 Wing Geometry Modification 16

1.4.2 Electromagnetohydrodynamic (EMHD) Flow Control 17

1.4.3 Mechanical Wingtip Devices 18

1.4.4 Simple Flat End Plates 18

1.4.5 Blended Winglets 19

1.4.6 Shifted Downstream Winglet 20

1.4.7 Evolution of Existing Designs 21

1.4.8 Proposed Design 23

Chapter 2: Design and CAD Model 23

2.1 Design Parameters and Range 23

2.1.1 Parameterized Geometry and Constraints 23

2.1.2 Range of Parameters 24

Chapter 3: Numerical Analysis 25

3.1 Computational Fluid Dynamics (CFD) and Ansys Fluent 25

3.1.1 Governing Equations in Fluent 26

3.1.2 Solvers and Linearization 27

3.1.3 Discretization Scheme 28

3.1.4 Shear-Stress Transport and Standard k- ω Turbulence Model 29

3.1.5 Wall Functions or Near-Wall Model 30

3.2 CFD Analysis and Problem Formulation 30

3.2.1 Two-Dimensional Analysis of Winglet Airfoils 30

3.2.4 ANSYS Fluent Case Setup 34

Chapter 4: Optimization 34

4.1.1 Response Surface Methodology 35

4.1.2 Optimization Constraints 35

Chapter 5: Design Validation 36

5.1 Experimental Validation 36
5.1.1 Principles of Modeling and Similitude *37*
Chapter 6: Cost Analysis **39**
Conclusions **39**
References **40**

List of Figures

Timeline **6**
Responsibilities **6**
Figure 1: Airfoil Parameters [15] **10**
Figure 2: Kutta-Zhukowsky Condition, Inviscid Flow [] **11**
Figure 3: Kutta-Zhukowsky Condition, Viscous Flow [] **11**
Figure 4: Starting Vortices [] **12**
Figure 5: Pressure Distribution Over an Airfoil [] **13**
Figure 6: Flow Separation and Vortex Formation for Post Stall Condition [] **14**
Figure 7: Vortex Configuration [] **15**
Figure 8: Superposition of Horseshoe Vortex in Steady Flow [] **15**
Figure 9: EMHD Configuration for Plasma Actuation [6] **17**
***Figure 10: Effects of Plasma Winglets and Configuration on Vortex Formation* [6]** **17**
***Figure 11: Force Balance on a Wingtip Device* [7]** **18**
***Figure 12: Flat End plates on Left: 747-400 – Right: A340-200* [7]** **19**
Figure 13: Winglet Parameters [16] **20**
***Figure 14: Wingtip Fence: Left: Airbus A380 – Right: A319* [7]** **20**
Figure 15: Wingtip Fence and Blended Winglet Comparison [18] **21**

Figure 16: Split Scimitar Winglets by Aviation Partners Boeing [17] 22
Figure 17: Scimitar Wingtip Cap [] ..... Error! Bookmark not defined.
Figure 19: Pressure (left) and Density (right) Based Iteration Scheme [7] 28
Figure: Wall Function Vs. Near-Wall Model Approach [7] 30
Figure: XFOIL Analysis of PSU 90-125WL Airfoil 32
Figure 18: Response Surface 35
Figure 1: Experimental Testing vs. CFD Analysis [20] 36

List of Tables

Table 1: Fenced-Wingtip Winglet Parameters 24
Table 2: Parameters for Lame Curve 24
Table 3: Range for Each Parameter 25
Table 4: Operating Conditions for Winglet 31
Table 5: Cost Breakdown 39

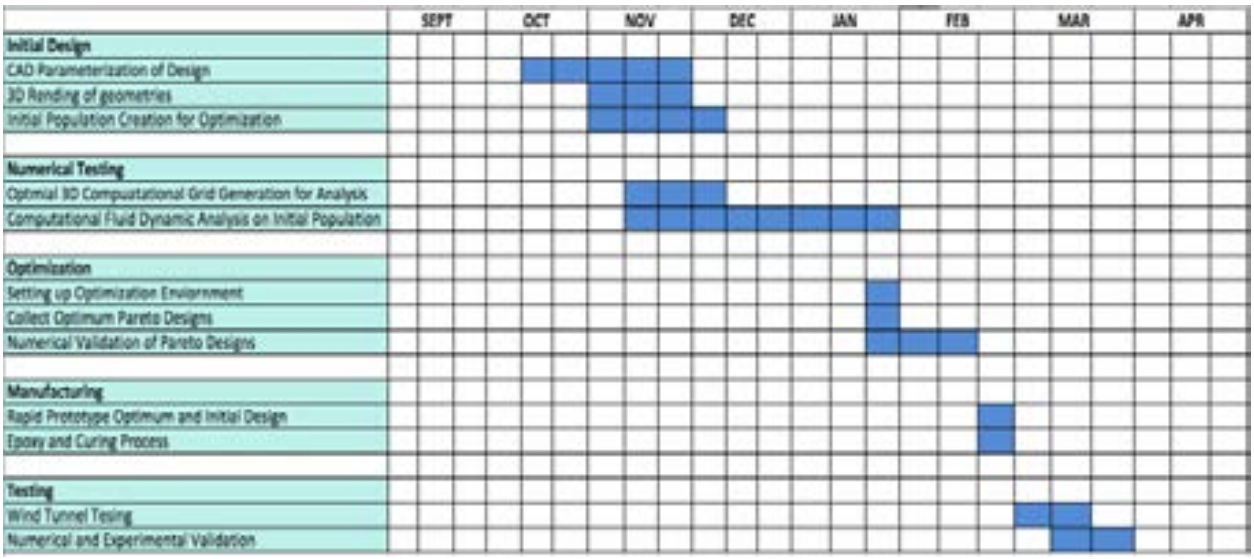

Timeline

	Sohail Reddy	Shanae Powell	Abraham Neiss
Research			
3D Rendering			
CFD Analysis			
Optimization			
Manufacturing			
Testing			

Responsibilities

Abstract

The problem being addressed here is design, analysis, multi-objective constrained optimization, construction and experimental validation of multi-winglets. The main purpose of this report is to formulate an optimization procedure for a design that reduces computational cost while producing an optimum design. The optimization is carried out using a Response Surface Approximation with twelve design parameters and two objective functions. The optimum winglet was tested at the Embry-Riddle's subsonic wind tunnel to compare experimental and computational results. The objective of this report includes design and optimizing a multi-winglet configuration capable of increasing the lift-to-drag ratio by 2% with respect to the currently implemented blended winglets used.

Chapter I: Introduction

1.2 Problem statement

Due to the constant increase in fuel costs, improvement in aircraft efficiency is necessary to maintain profitable and a stable aviation industry. The improvements via the addition of winglets and winglet configurations have been implemented to various degrees of successes. A further optimization of a new breed of winglets configurations can increase the efficiency of the aircraft.

The purpose of this project is to further optimize an existing design of winglets, with slight, cost effective modifications. The specific sets of winglets being optimized are the multi-winglets. To see the benefits of modification, the Boeing 757-200 wing will be studied. This commercial aircraft will be considered at normal cruising speed of Mach number 0.8 and altitude of 35,000ft since fuel efficiency is more desired at this segment of the mission profile. The goal of this project is to increase the efficiency of the blended winglets by 2%, which can lead to two hundred million dollars ($200,000,000) of savings in jet fuel cost.

1.2 Motivation

Due to the nature of pressure distributions and pressure leakages that occur when an airstream is confronted with a solid mass, in this case a wing, several challenges arise that need to be addressed. The predominant obstacle is maintaining a workable lift to drag ratio. The second challenge being to maintain the least turbulence conditions or minimizing the separation of laminar layers in the airstream around the airfoil. Due to the nature of continuity, the pressure gradient will try to diverge to zero as soon as it can. This can be seen when compressed air is diffused from a compressed air tank how higher pressure gas rushes to the atmospheric pressure conditions with a high velocity. This being the case, the consequential induced drag can inhibit forward thrust and minimize the range of flight. This situation creates a need for additional power to be generated by the engines in order to maintain proper flight conditions. This translates into more fuel consumption, which is a primary constraint in the aerospace industry, where fuel as a commodity has a fluctuating price tag, which has a trend of getting higher rather than lower. This market condition directly transcends into consumers paying more for flight expenses and the delivery of goods.

More fuel consumed leads to greater emissions of noxious gasses such as carbon monoxide and nitrogen oxide, which creates a greater carbon footprint and pollutes the environment. As engineers, we seek alternative more efficient methods daily. Sustainability practices and conserving of our environment has become one of our leading concerns. Therefore we are addressing this issue as well.

Another condition that has challenged modern air travel is the effect larger aircraft have on smaller craft during takeoff and landing in congested busy airports. Trailing vortices that are induced at the wings edges due to the divergence of the pressure gradient to equilibrium (namely zero) have veered other aircraft off course and worse have caused them to lose balance and crash. This condition creates the need to schedule gaps in aircraft landing and taking off. This additional constraint minimizes the traffic volume in a given airstrip or airport. This incurs more costs to air carriers since they cannot turn their craft around as fast. It also can affect military jets especially on aircraft carrier battle groups. Since multiple launches of fighters may be necessary in a combat situation. And the time restriction of launchings translates into smaller squadrons supplying air cover.

From an environmental standpoint, noise pollution especially from commercial airliners with two to four powerful engines can be a nuisance and a cause for higher penalties to airports from their local municipalities can become an additional financial burden on the costs associated with air travel.

In this project the Boeing 757-200 wing will be optimized with various winglet configurations and with slight, cost effective modifications to the existing design. The goal being that with the addition of these winglet configurations, a greater amount of efficiency namely increased range, a reduction of fuel consumption and safer and steadier flying conditions will be realized. This will benefit the consumer and the environment in tandem.

1.3 Literature Review

Over decades, with so many computational codes and software, such as Fluent, Nastran and OpenFOAM, it has become less difficult to predict aerodynamic properties of shapes. However, for efficient analysis in Computational Fluid Dynamics (CFD), one must have a firm understanding of the underlying concepts and theories involved in Fluid Mechanics. It is on this foundation, that we will construct our models and designs.

1.3.1 Theories of Lift and Drag

The lift on any aircraft is primarily generated by a two-dimensional cross section known as the airfoil, shown in Figure 1. Figure also shows the different parameters that can be defined to create specific airfoil geometry. The pressure difference over the lower surface and the upper surface of the wing results in a force perpendicular to the direction of the free stream velocity.

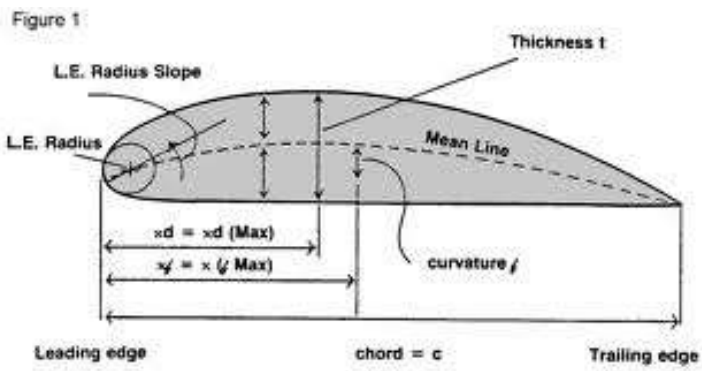

Figure 1: Airfoil Parameters [15]

1.3.2 The Kutta-Zhukowsky Condition

The Kutta-Zhukowsky Theorem, first developed its key ideas in the early 20th Century, finds a relationship between the lift generated by a shape, and the speed of the shape through the fluid, the density of the fluid, and the circulation. The circulation is defined as a closed loop integral of the velocity tangent to the around the airfoil shape. The theorem states the Lifting Force (L) per unit span is equal to the product of free stream density (ρ_∞), velocity (V_∞) and circulation (Γ), as shown in equation.

$$L' = -\rho_\infty V_\infty \Gamma,$$

It has been shown, that when an airfoil with a sharp trailing edge is moving through a fluid, the viscosity of the fluid causes the flow over the upper and lower surface of the wing to merge smoothly at the trailing edge. This establishes the Kutta-Zhukowsky condition, summarized as: A body moving through a fluid, will create about itself circulation of sufficient strength to move and hold the rear stagnation point at the trailing edge for a finite angle to make the flow about the trailing edge smooth. For a body with a blunt trailing edge, where the upper and the lower surfaces meet tangentially, equal velocities in the tangential direction on both sides are needed to establish a smooth flow.

As mentioned before, fluid's viscosity moves the stagnation points towards the trailing edge. Hence body moving through an invsicid fluid, fluid in which the viscosity is zero, does not create any circulation about itself. This causes the rear stagnation point to occur over the upper surface of the

body. The stagnation point position for both inviscid and viscous flow is demonstrated in Figure 2 and Figure 3.

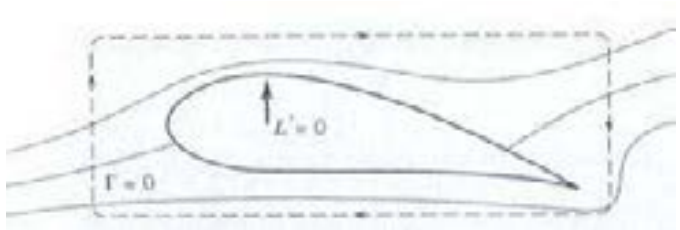

Figure 2: Kutta-Zhukowsky Condition, Inviscid Flow []

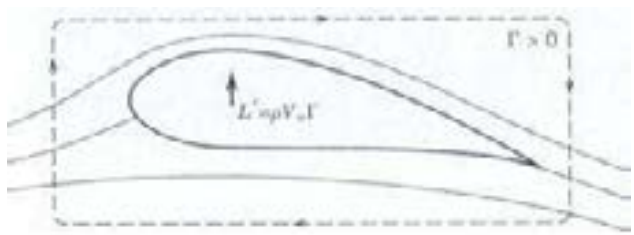

Figure 3: Kutta-Zhukowsky Condition, Viscous Flow []

1.3.3 Helmholtz Laws

In Fluid mechanics, Helmholtz's Law, is used to describe the three-dimensional motion of fluid in proximity of vortex filaments. This theory, in particular is applicable to inviscid flows and where viscous forces are negligible. The Helmholtz's Theorem are as follows [19]:

- Helmholtz's First Theorem
  - The strength of the vortex filament along its path is not changing
- Helmholtz's Second Theorem
  - Fluid particle, part of a vortex line, always belongs to the same line and therefore have the same vorticity. It also states fluid that is initially non-rotational remain irrotational
- Helmholtz's Third Theorem
  - The vortex filament must form a closed loop or must end at the boundaries.

Based on Helmholtz's Second Theorem, the total circulation around a body must remain constant. Since the initial total circulation around a body at rest in a fluid is zero, it must remain zero once the object is in motion. To satisfy both the Helmholtz's Third Theorem and the Kutta-Zhukowsky condition, the formation of "starting vortices" , shown in Figure 4,are required.

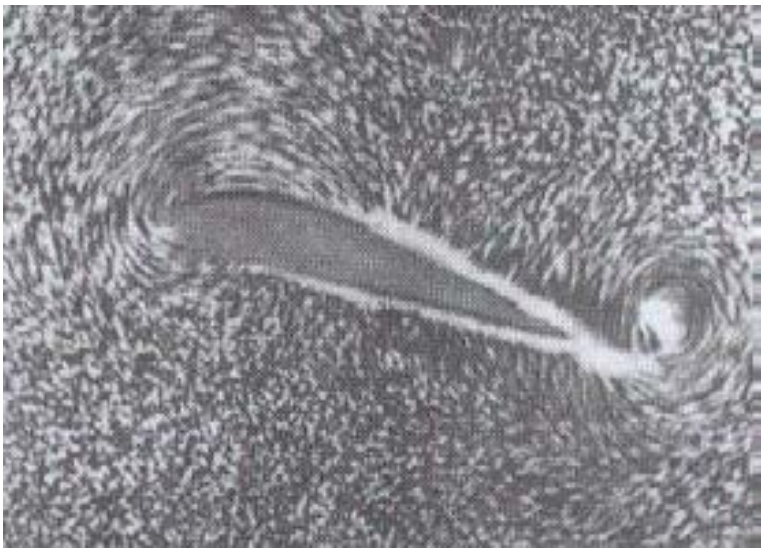

Figure 4: Starting Vortices []

The starting vortices create circulation equal and opposite to that around the airfoil. The induced flow due to the vorticity of the airfoil and the starting vortices is needed to obtain a smooth flow at the trailing edge. It can also be seen from Figure 4, the increase in speed of the fluid at the leading edge. This increase in velocity results in a decrease in pressure over the upper surface of the airfoil, which in turn leads to a "leading edge suction" phenomenon. This basic principle of having a pressure difference between the upper and the lower surface leads to the creation of lift.

This pressure difference is present over the entire chord length of the airfoil. Figure 5 shows a typical pressure distribution over an airfoil surface. The arrows show pressure vectors. As it can be seen, an airfoil produces a force perpendicular to the chord line, known as lift, and parallel to the chord line, known as drag.

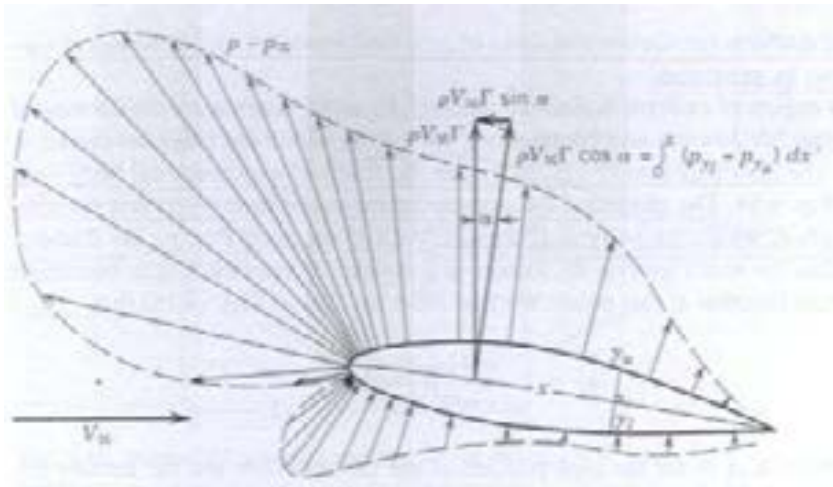

Figure 5: Pressure Distribution Over an Airfoil []

In a perfect fluid, inviscid fluid, the total lifting force can be represented as

$$L=\rho V_{\infty} Cos\ \alpha$$

The drag force can be represented as,

$$D=\rho V_{\infty} Sin\ \alpha,$$ where α is known as the angle of attack.

The entire pressure distribution can be integrated over the entire chord length to obtain total forces acting on the airfoil. In viscous fluid, the pressure distribution is altered due to the generation of viscous drag.

1.3.4 Stall Characteristics of Airfoils

It can be seen from the equations for lift and drag, that the forces are dependent on the angle of attack. As the angle of attack increase, so does the lifting force. This relationship remains true until the stall angle is reached. An airfoil in post stall conditions experiences violent flow separation, leading to very high drag forces and a sudden loss in the lifting force. The flow separation is due to the adverse pressure gradient, leading to reversal of velocity profile in the boundary layer and therefore leading to boundary layer separation. At large angles of attack, the Kutta-Zhukowsky condition no longer holds, thus leading to the formation of large vortices, as shown in Figure 6.

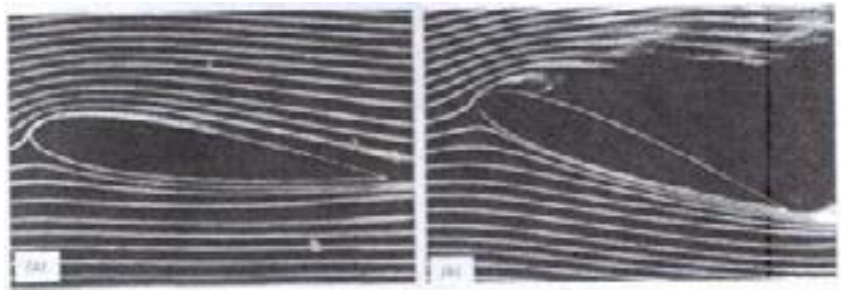

Figure 6: Flow Separation and Vortex Formation for Post Stall Condition []

1.3.5 The Finite Wing Theory

A computational model must closely resemble the realistic geometry under investigation. Any wing in three dimension has a finite wingspan, and therefore a separate theory must be developed for explaining the three dimensional phenomenon. The Airfoil-Vortex analogy helps forms the platform for understanding and calculating properties of finite wings.

1.3.6 Flow Field Around Finite Wings

The flow field around a finite wing is much different than the flow field around a wing with an infinite wingspan, i.e. an airfoil. A combination of both Helmholtz's Second Theorem and the Kutta-Zhukowsky can be used to explain a unique phenomenon for a finite wing.

Consider a wingspan b, in a uniform free stream flow of velocity V_∞ and constant circulation Γ; as stated by the Kutta-Joukouski condition, the force felt by the vortex is equal to $V_\infty \rho \Gamma$ and is perpendicular to V. Helmholtz's Second Theorem does not allow the bound vortex to end at the wingtips; it requires it to form a complete circuit or extend to infinity.

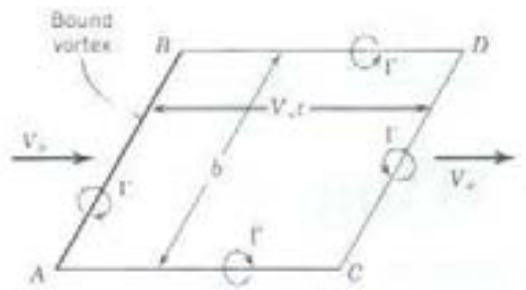

Figure 7: Vortex Configuration []

In Figure 7, side AB represents the leading edge, CD represents the trailing edge, and AC and BD are the wingtips. As the wing moves through the fluid it forms starting vortices about AB and CD of equal magnitude but opposite circulation. The trailing tip vortices of magnitude Γ about BD and AC satisfy all of Helmholtz's Theorems.

It is also stated, that the velocity that is induced by a given vortex decreases as you move away from the vortex. The starting vortices usually reside, with time, from the wing position and soon become negligible compared to those induced by the portions of trailing tip vortices near the wingtips. A head on view of Figure 8 can help visualize the formation of trailing tip vortices.

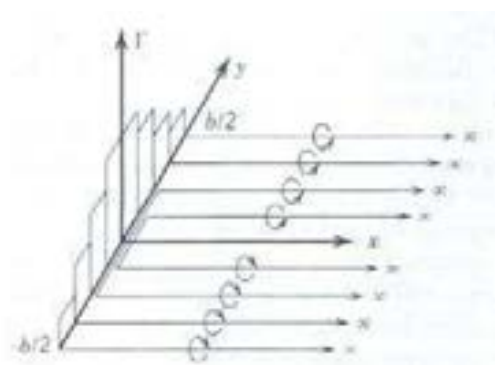

Figure 8: Superposition of Horseshoe Vortex in Steady Flow []

1.4 Methods of Induced Drag Reduction and Retardation of Vortex Formation

As mentioned before, vortices are formed when the high pressure from the underside leaks around the wingtips to the upper side. Since aircraft wings are finite and not infinite, at the wingtips, it causes this phenomenon to occur. It has also been stated that vortices increase induced drag by creating downwash at the wing. These not only increase drag on a wing, but also decrease its lift.

1.4.1 Wing Geometry Modification

One method of dealing with this problem is to increase the aspect ratio of the wing. The aspect ratio, AR, equation below,is defined as the ratio between the square of the wingspan, b, and the area of the wing planform, S.

$$AR = \frac{b^2}{S}$$

A higher aspect ratio yields a lower pressure gradient between the upper and lower side of the wing over a larger wingspan. Due to this decrease gradient, the vortices formed at the wingtip are weaker, leading to less induced drag. This increase in wingspan, however, gives rise to higher bending moment at the root. This can lead to structural fatigue and eventual failure of the structure.

The second modification made to the wing itself includes increasing the taper ratio. The taper ratio is defined as the ratio of the root chord length to the wingtip chord length. This allows the wing to produce the same overall lift further inboard, closer to the root. This allows for shorter chord length toward the wingtips, which results in smaller pressure difference between the upper and lower surface of the wing. This results in vortices of lesser strength and a decrease in induced drag.

This reduction in chord length towards the wingtip makes the wingtip fragile. The area closer to the wingtip experiences immense loads due to the pressure gradient alterations due to the implementation and use of control surfaces. Therefore this area of the wing needs to be structurally strong, which, when the higher taper ratio constraint is exercised, would result in a heavier wing structure. A stronger wing structure require an excessive use of stingers, ribs and longerons, which reduces the volume of the housed fuel tank, and increase the overall weight of the aircraft.

1.4.2 Electromagnetohydrodynamic (EMHD) Flow Control

A second, more unconventional, method of retarding vortex formation can be by means of implementation of electromagnetohydrodynamic (EMHD) flow control, configuration for which is shown in Figure 9.

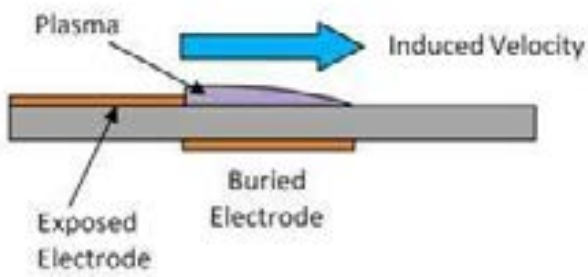

Figure 9: EMHD Configuration for Plasma Actuation [6]

This makes use of plasma actuators, electrodes, to create plasma, weakly ionized air. Applying a sufficient electric potential, to these electrodes creates an electric field in between them. If the voltage applied exceeds the breakdown voltage of the air, which is about 3000V, or if the electric field strength exceeds 3000000 V/m, the air is ionized to form plasma. This plasma, once in the electric field, feels a Lorentz Force, in the direction of the electric field lines. This can be used to redirect flow separation and reduce the strength of the vortices formed. Figure 10 shows the visual effects of such plasma actuators placed at wingtips, and it is clear to see the benefits. According to Jacob's wind tunnel results, Plasma winglets show a 92% increase in lift along with a noticeable change in the vortex structure [6].

.

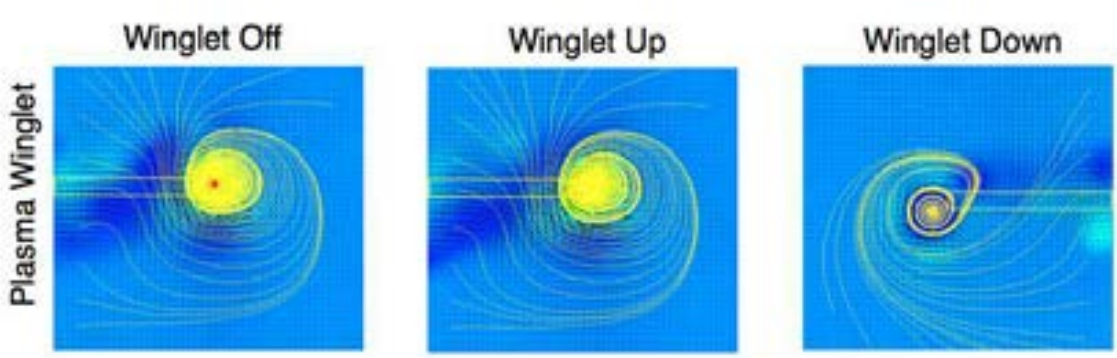

Figure 10: Effects of Plasma Winglets and Configuration on Vortex Formation [6]

1.4.3 Mechanical Wingtip Devices

The next set of modification that can be made involve the use of solid surfaces to interact with the flow field to decelerate and weaken the vortex. Few advantages of using such devices include an effective increase in wingspan and therefore the lifting force, a decrease in induced drag through redirection of the flow to minimize vortex formation. As seen in the Figure 11, proper design of winglets, through use of their airfoil shape, can indeed be used to produce an additional thrust force. This phenomenon can be produced in any of the below winglet designs.

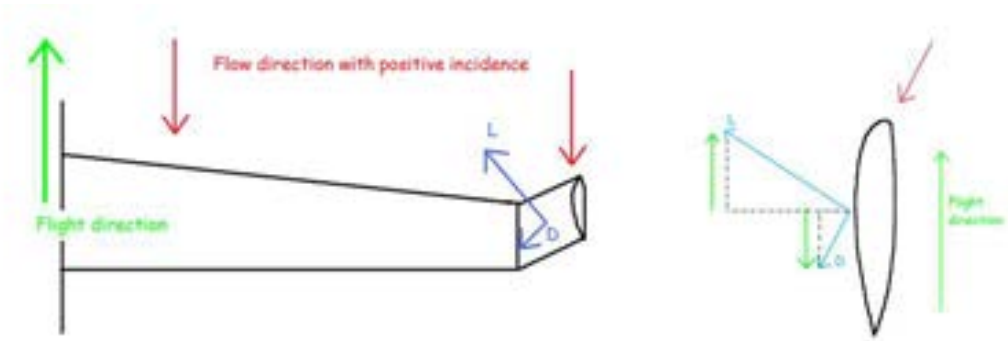

Figure 11: Force Balance on a Wingtip Device [7]

1.4.4 Simple Flat End Plates

A third method to decrease induced drag due to vortices is to use end plates. Although it is impossible to stop the fluid rotation, it is possible to decelerate it. Figure shows two examples of such endplates. This approach is seen as an addition of a wingtip device “without care”, i.e. a universal design used to give improved performances rather than optimized, best possible performance.

Figure 12: Flat End plates on Left: 747-400 – Right: A340-200 [7]

As it is seen in Figure 12, the point where the base of the winglet and the wingtip meet, forms a sharp angle. This can cause the boundary layer of the circulation flow to be subjected to adverse pressure gradient. This adverse pressure gradient then causes a secondary smaller auxiliary vortex to form at this connection point [7]. This method does reduce the strength of the primary vortex but leads to the formation of an auxiliary vortex. Due to this, the overall induced drag is reduced but not optimized for the best possible performance. Benefits of such design are the low cost of manufacturing and retrofitting, as a base design can be used on any aircraft with minimal adjustment to the initial wingtip.

1.4.5 Blended Winglets

As the name suggests, this form endplate features a smooth transition between the wing and the end plate. Since this design is perfectly fitted to the wing, the sharp connection point between the wing and the plate is avoided, leading to the elimination of the auxiliary vortex formed from the adverse pressure gradient. In 1994, Grazter introduce the blended winglets, a design to reduce interference drag. Interference drag is a phenomenon cause by the intersection of lifting surfaces.

Winglets that lie perfectly in the plane of the wing, increases the effective wingspan of the wing thus increasing the lifting force. This however has the same disadvantages as an increase in aspect ratio, where as the increase in lifting force at wingtip cause an increase in bending moment at the root. Due to this winglets generally lie in the mid plane, defined by the cant angle, to both the vertical and the

horizontal plane. This ensures the mixture of both increased lift and reduced induced drag. Figure 13 shows the various parameters that are used to define the shape of the winglet.

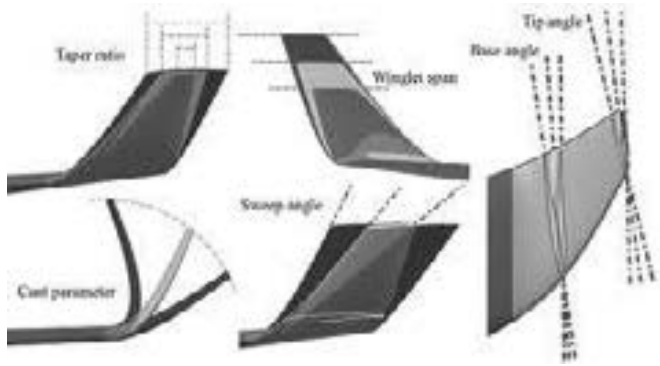

Figure 13: Winglet Parameters [16]

1.4.6 Shifted Downstream Winglet

As mentioned before, the downfall of having a vertical endplate is the formation of the auxiliary vortex. This can be overcome using a blended winglet but that proposes an increase in bending moment about the root, due to the increase in effective wingspan. The form of wingtip device that eliminates the pitfalls of both of the above-mentioned devices is known as a "Wingtip Fence", shown in Figure 14.

Figure 14: Wingtip Fence: Left: Airbus A380 – Right: A319 [7]

The wingtip fence design too has a sharp meeting point between the wing and the wingtip device, but due to the downstream sweep of the end plates. This reduces the adverse pressure gradients and therefore the risk of flow separation [7].

Figure 15: Wingtip Fence and Blended Winglet Comparison [18]

It can also be seen from Figure 15, that the wingtip fence, in comparison to the blended winglet, is rather small in size. This not only reduces the weight of the overall structure and the manufacturing cost but also decreases the bending moments produced at the root. Due to the nature of the wingtip fence, no alteration has to be made to the wingtip, since the fence does not cover the entire wingtip. This allows for a lower taper ratio, where the wingtip chord is larger thus producing more lift over the entire wingspan.

1.4.7 Evolution of Existing Designs

Seeing the effects winglets have on the efficiency of the aircraft, designers are constantly searching for better alternatives. This can be through complete redesign of the winglets or modification of the existing one. This has been seen in the year 2013, where both Boeing and Aviation Partners introduced a new design. This new concept combines the lower extrusion feature of the fenced tip and the smooth connection of the blended winglet. Named after a curved backsword, the scimitar winglets,

Figure 16, feature a split design with an upward and a downward facing winglet. This again increases the effective wingspan therefore further increasing the lift.

Figure 16: Split Scimitar Winglets by Aviation Partners Boeing [17]

The scimitar winglets, current in the testing phase, made its maiden test flight on July 16th, 2013 on the wingtips of a United Airlines Boeing 737-800. Due to the recent release of this design, very little is known about the scimitar winglets. Recent testing by Aviation Partners Boeing suggests that the Split Scimitar Winglets will results in approximately 2% fuel savings for any 737 fitted with it, saving them more than $200 million per year in jet fuel costs, which again leads to a reduction in carbon emissions.

As with any design, the positives must far outweigh the negatives. In the case of winglets, the performance increase in efficiency must be greater than the cost of manufacturing. This design manages to do that by updating an already existing blended winglet design by retrofitting a Scimitar tipped ventral strake. Therefore only there ventral strake has to be manufactured thereby reducing manufacturing cost and time.

1.4.8 Proposed Design

In the constant search for improved performance, engineers must continue development in their designs. The proposed goal of this project is to further optimize multi-winglets. This allows for direct comparison between multi- winglets and the ordinary blended winglets.

The blended winglets have been optimized before for a senior thesis in 2010 at Florida International University, which featured a 2.43% increase in the Lift-to-Drag ratio from the base design used by Boeing in the 757-200. Optimizing the Scimitar Wingtip Cap for this blended winglet allows for better comparison, as the data is readily available, while reducing both computational cost and experimental cost. The same wing profile was considered to keep the pressure distribution over the surface of the wing the same in all testing environment.

Chapter 2: Design and CAD Model

2.1 Design Parameters and Range

With any optimization goal, the variables of the design must be clearly outlined. These parameters define the geometry and allow for the modification of it. The optimization run will provide a design with optimal combination of values for each parameter.

2.1.1 Parameterized Geometry and Constraints

An efficient way to define the geometry is necessary to reduce computational cost and computational time. If the parameters can be related to one another, it drastically reduces the number of input variable, thus leading to a smaller initial population needed for the optimization run (See Response Surface Methodology).

A total of seven design variables, shown in table _, have been used to define the wingtip-fenced winglets.

Table 1: Fenced-Wingtip Winglet Parameters

α	Leading Edge Sweep Angle
L_L	Leading Edge Length
β	Trailing Edge Sweep Angle
L_T	Trailing Edge Length
S	Winglet Span
Δx	Position from Wingtip Leading Edge
L_U	Upper Vertical Length
L_V	Lower Vertical Length
λ	Lame Curve

The lower leading edge curve is defined by using the lame curve, equation []. The coefficients a,b and n are defined in table 2. Here, one constraint put on the design parameters is that the Ellipse Vertical Length is equal to the Lower Vertical Length. The second constraint on the overall design is that the leading edge and trailing edge height, for both the upper and lower part, are equal.

$$\left|\frac{x}{a}\right|^n + \left|\frac{y}{b}\right|^n = 1$$

Table 2: Parameters for Lame Curve

a	Ellipse Horizontal Length
b	Ellipse Vertical Length
n	Lame Exponent

2.1.2 Range of Parameters

The optimization run will provide optimized values for the parameters used to define the geometry. These optimum values obtained fall within the range of the values for the initial population.

For this a good range must be defined for each of the design parameters. Without an established range, the values for the each of the design parameters could range from negative infinity to positive infinity. This established range is usually constrained by other components that the design will interact with. Table 3 shows the allowable range for each parameter for the fenced-tip winglet.

Table 3: Range for Each Parameter

Lower Limit	Parameter	Upper Limit
	α	
	L_L	
	β	
	L_T	
	S	
	Δx	
	L_U	
	L_V	
	λ	

Chapter 3: Numerical Analysis

It is important to find the effects of each winglet design to see how it compares to other designs. This can be done both experimentally and by means of simulations, computationally. Since experimental testing requires manufacturing of each design, the computational analysis is a more attractive choice. This computational analysis, known as Computational Fluid Dynamics (CFD), will be carried out using a finite volume solver, Ansys Fluent.

3.1 Computational Fluid Dynamics (CFD) and Ansys Fluent

Computational Fluid Dynamics is a branch of computational physics that involves the use of numerical methods and algorithms to compute solutions to problems involving fluid flows. This involves the use of computers to solve the system of governing equations that define the physics, in this case the

Navier-Stokes equations, and thus simulate the dynamic interaction between the surface and fluid defined by prescribed boundary and initial conditions. Fluent software is one of many commercial solvers that uses finite element discretization to solve the system of equations. The basic steps for obtaining the flow field are the following:

- Define geometry
- Define and discretize (split into mesh cells) the fluid volume around the geometry
- Physical model is defined – states the governing system of equtions
- Boundary and Initial conditions are defined
- Solver solves the governing systems of partial differential equations
- Visualization software used to view the results

3.1.1 Governing Equations in Fluent

The governing equations are defined by the physics of the problem. In CFD analysis of the winglets, Fluent will solve three governing equations. These include equations for conservation of mass, momentum and energy.

The conservation of mass, or the continuity equation can be written is as follows:

$$\frac{\partial \rho}{\partial t} + \nabla \cdot \left(\rho \vec{V}\right) = \dot{m}$$

,where ρ is fluid density, t is time, $\vec{V}$ is flow velocity vector, and $\dot{m}$ i is the mass generation.

The conversation of momentum, Navier-Stokes equation, can be written as follows:

$$\frac{\partial (\rho \vec{V})}{\partial t} + \nabla \cdot \left(\rho \vec{V}\vec{V} - \underline{\underline{T}}\right) = \rho \vec{b}$$

,where $\underline{\underline{T}}$ is the deviatoric stress tensor and $\vec{b}$ is the body force, per unit volume.

The conservation of energy equation can be written as follows:

$$\frac{\partial(\rho e_o)}{\partial t} + \nabla \cdot \left(\rho e_0 \vec{V} - \underline{\underline{T}} \cdot \vec{V} + \dot{\vec{q}}_c + \dot{\vec{q}}_r\right) = \rho \vec{V} \cdot \vec{b} + \rho \dot{q}$$

3.1.2 Solvers and Linearization

Fluent has two types of built in solvers, density-based and pressure-based solvers. In both methods, the Fluent solves the governing set of equations using a control volume based technique. This involves the division of the computational domain into discrete control volumes, integration of the set of governing equation on the individual control volumes, and then linearization of discretized equations and solutions (see discretization methods).

The pressure-based solver solves the governing set of equations sequentially. Since each of these equations is non-linear, they require more than one iteration before they converge. At each iteration, several distinct steps are run. These steps are shown in Figure _ (for more information about each step, please refer to the Fluent User's Guide).

A density-based solver solves the set of equations at the same time. Even though the iteration scheme, Figure _, for density-based solver is smaller, the convergence time is longer. The pressure-based solver is used mainly for low speed flows, where the flow can be assumed to be incompressible, while the density-based solver is better for high-speed flows.

The non-linear equations, in both solvers, are linearized by either implicit or explicit scheme. Implicit scheme is where the unknown values are found using both known and unknown values from neighboring cells. In this case, each unknown appears in more than one equation and the system of equation is solved at once. Explicit scheme is where the unknown values are found only from known values. In the pressure-based solver, the user has no choice between implicit or explicit scheme.

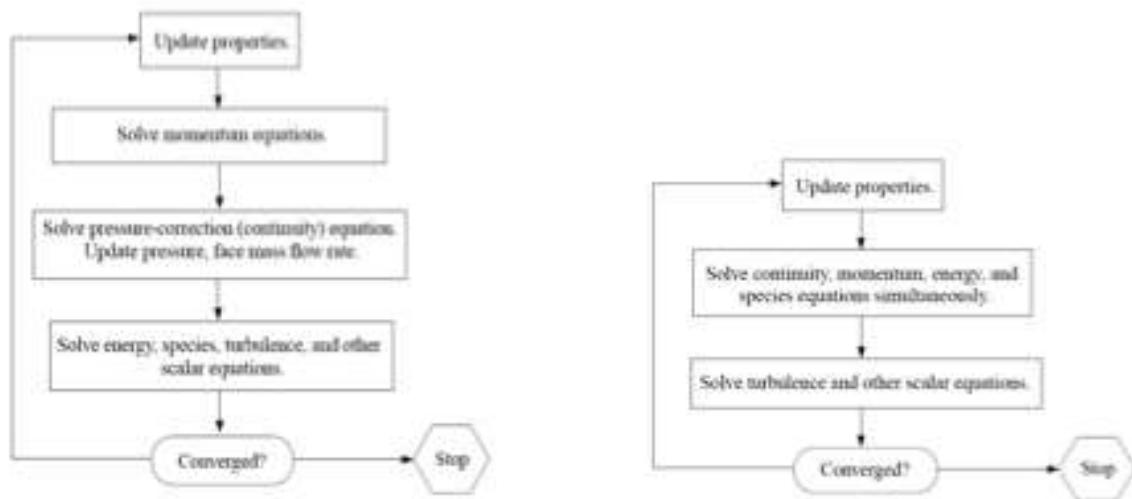

Figure 19: Pressure (left) and Density (right) Based Iteration Scheme [7]

3.1.3 Discretization Scheme

Fluent uses a finite volume method to divide the entire domain into little control volumes. It then integrates the entire volume governing equations, thus giving a discretization of the whole domain. By default, Fluent stores the value of Φ for each cell at its center, where Φ is any scalar parameter whose transport is being calculated. This is all acceptable, but to calculate convection terms, the face values, Φ_f are needed.

To find these Φ values, fluent interpolates values from cell centers in different ways named upwind schemes. The word "upwind" refers to the values being computed thanks to the upstream cells, according to the direction of the normal velocity. The two schemes used in Fluent are First-Order Upwind and Second Order Upwind.

In the First-Order scheme, the values of Φ_f are assumed to be the same as the value of Φ at the cell center. In the Second-Order scheme the values of Φ_f are computed with a multidimensional linear reconstruction approach. This is done by means of a Taylor series expansion of the cell-centered solution. The equation to calculate the face value, Φ_f, is shown below, where Φ is the cell-centered value, $\nabla\Phi$ is its gradient, and Δs is the distance from the upwind cell centroid to the face centroid.

$$\phi_f = \phi + \nabla\phi \cdot \Delta\vec{s}$$

3.1.4 Shear-Stress Transport and Standard k- ω Turbulence Model

Turbulence modeling is very important in simple fluid flow, since viscous strength and therefore viscous drag is a relevant component of total drag. The turbulence model chosen for this case was the Shear-Stress Transport (SST) k-ω model. This model is based on the Wilcox k- ω model that especially dedicated for modeling waves, mixing layers and plane, round and radial jets. It is typically designed for boundary layers resolution.

A variation to this model, SST k-ω model, was developed to combine the robust and accurate standard k-ω model in the near-wall region with the k-ε model in the far field. The k-ε model is a two-equation model that gives a solution to each transport equation. These solutions allow one to independently determine the turbulent velocity and the length scales.

This model solves two transport equations for k and ω, which are turbulence kinetic energy (TKE) and the turbulence dissipation rate (TDR) respectively. The equations they are obtained from are shown below,

$$\frac{\partial}{\partial t}(\rho k) + \frac{\partial}{\partial x_i}(\rho k u_i) = \frac{\partial}{\partial x_j}\left(\Gamma_k \frac{\partial k}{\partial x_j}\right) + G_k - Y_k + S_k$$

$$\frac{\partial}{\partial t}(\rho \omega) + \frac{\partial}{\partial x_i}(\rho \omega u_i) = \frac{\partial}{\partial x_j}\left(\Gamma_\omega \frac{\partial \omega}{\partial x_j}\right) + G_\omega - Y_\omega + S_\omega$$

where, $\boldsymbol{G_k}$ is the generation of turbulence kinetic energy due to mean velocity gradients, $\boldsymbol{G_\omega}$ represents the generation of **ω**. $\boldsymbol{\Gamma_k}$ and $\boldsymbol{\Gamma_\omega}$ represent the effective diffusivity of **k** and **ω** respectively. $\mathbf{Y_k}$ and $\mathbf{Y_\omega}$ represent the dissipation of **k** and **ω** due to turbulence. The $\mathbf{S_k}$ and $\mathbf{S_\omega}$ are user-defined source terms [12].

3.1.5 Wall Functions or Near-Wall Model

It is well known that flow is affected by near by walls. Near these walls, the flow velocity decreases due to the no-slip condition enforced by the fluid viscosity. This boundary layer phenomenon significantly affects the numerical analysis. The k-ε model is valid in the far field and not so much in the near-wall domain. In the case of analysis of winglets, it is very important to model the near-wall effects accurately since the boundary layer of the airfoil heavily influences the characteristics of the wing.

To capture the boundary layer phenomenon accurately, a refined mesh is needed at the near-wall location. This is however increases the computational cost and time. When this region is not of any interest, wall functions are used. Wall functions acts as a kind of "black box" to bridge cells and the wall itself. This can be seen in Figure _. This approach is used for high Reynolds number, where the viscous effects can be considered negligible.

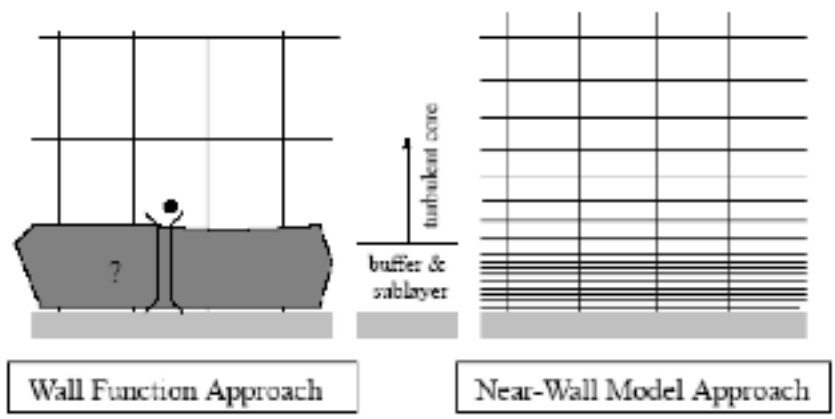

Figure: Wall Function Vs. Near-Wall Model Approach [7]

3.2 CFD Analysis and Problem Formulation

3.2.1 Two-Dimensional Analysis of Winglet Airfoils

One important feature of the winglet, that influences its performance, is the airfoil profile. As with general airfoil requirements, one of the main goals is to generate the most lift at the lowest possible drag. As shown before, drag is directionally proportional to the velocity squared; therefore it is

very imported to generate a low drag design. The coefficient of pitching moment, generally a design consideration for main wing, can be neglected for winglet design.

Mark Maughmer, Timothy Swan, and Steven Willits, at Penn State University, designed and tested an airfoil for winglet design. Their final design, the PSU 90-125WL airfoil, featured a low drag design with stable results throughout the operating range.

This airfoil was tested for our case in a 2D analysis code written by Mark Drela called XFOIL. XFOIL is used for analysis of subsonic isolated airfoils whose shape is defined by X and Y coordinates. It is able to compute the pressure distribution and coefficients of lift, drag and moment for that given airfoil, given the Mach Number, Reynolds Number and the Angle of Attack. The operating conditions at which the PSU 90-125WL airfoil was tested are shown in table_. XFOIL uses a panel method to model the outer potential flow. This potential flow is solved using an Euler solver, where the flow is assumed to be inviscid. The viscous effects in the boundary layer are accounted for by using an integral boundary-layer approach.

Table 4: Operating Conditions for Winglet

Mach Number	**0.8**
Altitude (m)	**11,000**
Density (kg/m^3)	**0.4135**
Absolute Viscosity (Ns/m^2)	**1.458x10^{-5}**
Approximate Reynolds Number	**13386283**

The characteristics of this airfoil closely meet our requirements. It can be seen in Figure_, that the PSU 90-125WL airfoil has a small coefficient of drag. Cd. The yellow and blue lines over the wing represents the streamlines over the upper and lower surface of the airfoil. The yellow and blue graph lines represent the viscous coefficient of pressure over the upper and lower surface. One contributing factor to such a low coefficient drag is due to the sustained laminar flow over the surface of the wing. This laminar bubble is shown in the pressure distribution graph as a sudden drop in pressure. This laminar bubble is created due to the laminar separation before it and the turbulent reattachment after it. XFOIL also notifies the user when the flow over the airfoil becomes supersonic. Flow turning supersonic over a surface results in a shockwave, which increases drag. The flow over the entire PSU 90-125WL airfoil is subsonic therefore not producing a shockwave.

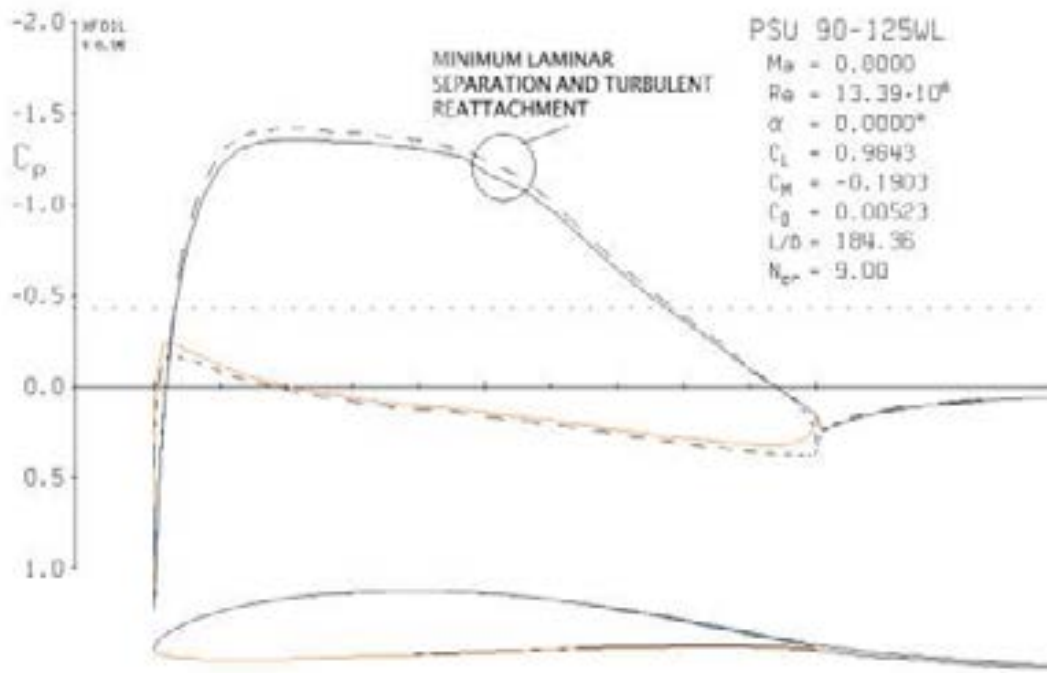

Figure: XFOIL Analysis of PSU 90-125WL Airfoil

In Figure_, the dotted line and the solid lines in the graph represent the inviscid and viscous coefficient of pressure. It can be seen that the two types of lines nearly overlap each other, indicating the viscous and inviscid coefficient of pressure are very similar. This is due to the high Reynolds Number the airfoil performed at. Reynolds number is the ratio between inertia forces and the viscous forces. The high Reynolds number indicates that the inertia forces far dominate the viscous forces, therefore the viscous forces are said to have negligible effect. The Reynolds Number, RE, can be calculated from the following equation, where ρ, v, l and μ is the density, velocity, characteristic length and dynamic viscosity.

$$RE = \frac{\rho v l}{\mu}$$

3.2.2 Finite Volume Method

As mentioned before, Fluent uses the finite-volume method (FVM) to solve the set of partial differential equations. FVM is used to represent and solve partial differential equation in the form of algebraic equations [21,22]. This involves evaluating these equations and computing values at discrete places on a meshed geometry. Each node point in the meshed geometry is enclosed in a small volume, hence the name finite volume. The volume integrals in the partial differential equations, in our case the Navier-Stokes equations, that contain the divergence term, ∇, are converted to surface integrals by means of the divergence theorem. The divergence theorem relates the flux of a vector field through a surface, to the behavior of the vector field within the surface. This allows the divergence terms to be evaluated as fluxes at the surface of each finite volume. The Finite-Volume method is a conservative method since the flux entering a control volume is equal to that leaving the adjacent control volume. The finite volume method also allows for computations on an unstructured grid or mesh.

3.2.3 Three-Dimensional Computational Grid Generation

The Finite Volume method requires that the computational domain be discretized into smaller domains. This discretization is known as meshing. As mentioned before, the finite volume method allows for computations using an unstructured grid, which is very attractive given the complex geometry. An unstructured grid follows no pattern around the domain where as a structured grid follows a pattern. It is also important to state that since the aerodynamic shape of the geometry is being optimized, the internal structure is being neglected. This reduces the number of mesh cells needed as only the surface of the geometry needs to be mesh and not the internal structure. The geometry meshing will be carried out in an automatic meshing software built into ANSYS.

ANSYS allows the user to control the mesh by changing mesh size, face size, bias, and inflation to name a few. It is known the quality of the mesh, mesh size, directly affects not only the results obtained but also computational times. A finer mesh leads to more accurate results but can be computationally and time costly. For this reason it is imperative to mesh the domain efficiently. One way to achieve both

accurate results and reduce computational cost is through mesh refinement, which is increasing cell density in area of high gradient. In the case of this analysis, it is known that around the wing, certain values such as pressure and velocity to name a few, will vary more from cell to cell than anywhere around the domain. This steep gradient in these parameters require for smaller mesh cells in this area whereas these values in the far field region are of less interest. This fact drives the mesh size to be smaller closer to the geometry, progressively getting larger as we move away from the wing.

Since the standard no-slip condition is being applied to the wing surface, the boundary-layer phenomenon must be taken into account. Even though the wing is operating at a high Reynolds number, it is fair to assume inviscid flow outside the boundary layer. However, within the boundary layer, the viscous forces are high and must be taken into account. The Near-Wall Model approach mentioned before is used, where the mesh cells are small closer to the surface of the wing.

3.2.4 ANSYS Fluent Case Setup

Having discussed the different factors that affect CFD analysis, the actual case setup and setting will be discussed. As mentioned before, the Density-Based solver is used to account for the compressibility at high Mach number, and Shear-Stress-Transport to model the boundary layer and flow separation. The Boundary Conditions are set at a Mach .8 at zero degrees at the inlet, zero pressure at the outlet, and the no-slip condition at the wing-winglet configuration. The fluid used is air, with user control viscosity, density to account for the altitude effects.

Chapter 4: Optimization

As mentioned before, there are many parameters that affect the performance of the winglets, such as Cant Angle, Wingspan, Taper Ratio and Sweep to name a few. Since the Navier-Stokes are highly non-linear, due to the convective acceleration term, it is almost impossible to obtain an analytical solution. For this reason a numerical solution must be obtained. It is also important, due to the computational cost of such analysis, that a robust optimization method be used to obtain an efficient design.

4.1.1 Response Surface Methodology

Due to the high computational, a more robust optimization technique is necessary. For this reason, the Response Surface Approximation is used as the method of choice. Response Surface Methodology creates a relationship between several input variables and one of more output variables. This relationship is shown as a three dimensional surface shown in Figure 18. This is done by supplying an initial population of design, the input and their respective outputs, to create the surface. The optimization environment uses these variables to "train" the response surface, interpolating between the data set and extrapolating outside the data set. This allows for investigation of objective functions outside of the range of initial population. The output variables that are being altered using the optimization technique are known as the objective functions.

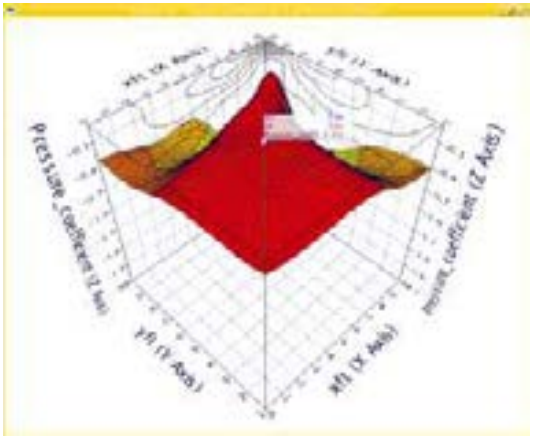

Figure 18: Response Surface

4.1.2 Optimization Constraints

As with any design consideration, allowable range of parameters must be defined. These are known as constraints, and they help keep the optimal design search within a user and physics defined range. At the moment, both parametric constraint and the constraints on the objective functions are not known, as further analysis of the initial design is needed.

Chapter 5: Design Validation

Even though computer simulations reduce the cost for designing a new product, experimental validation of the design is imperative. Experimental testing shows how the product will perform in the exact environment in which it will operate. It also allows for more accurate results as simplifications might have been used in the numerical analysis of the design. Figure _, compares the flow structure obtain from experimental testing and CFD analysis [20]. It can be seen that due to incorrect setting or simplification the flow separation isn't modeled exactly.

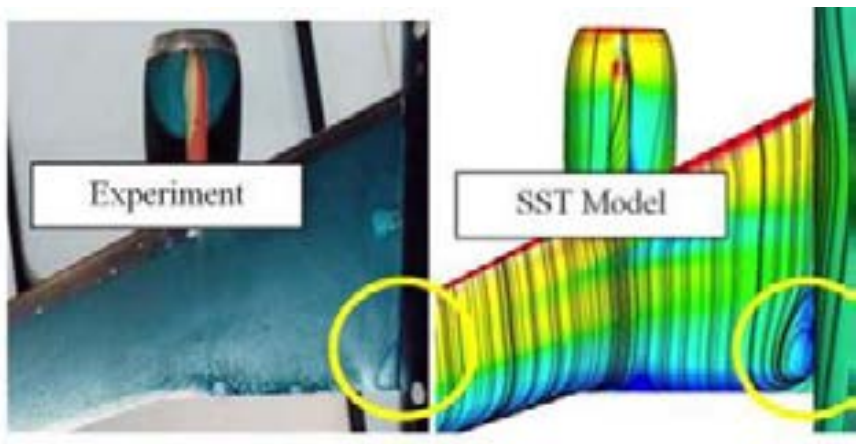

Figure 1: Experimental Testing vs. CFD Analysis [20]

5.1 Experimental Validation

In the case of fluid flow, the most common form of experimental validation is through Wind Tunnel testing. This involves placing the specimen in a tube where air is forced over the specimen and the needed data is recorded. For the purpose of testing our prototype, the wind tunnel at Embry-Riddle Aeronautical University was used as the testing facility.

5.1.1 Principles of Modeling and Similitude

When carrying out experimental testing in the wind tunnel, it is important to perform the experiment at the same conditions as the computational analysis. This is sometimes hard, if not impossible to do. In the case of this study, the prototype model will have to be to scale, fly at 35,000 ft, at .8 the speed of sound. This would require that the prototype be manufactured, fitted to the aircraft and all of the various license and testing documents be filled out.

Another method for testing prototype, at a smaller scale, is by applying the principles of Modeling and Similitude. This requires for the modifications of certain parameters so that phenomena at full scale testing and small scaled testing is the same. To see which and how parameters should be modified, the concept of Nondimensionalization must be applied. Nondimensionalization is a method of representing an equation by removal of units defining physical quantities. In the case of our study, the equation being nondimensionalized is the Conservation of Linear Momentum.

The Momentum equations for nondimensionalization can be written as

$$\rho \frac{D\vec{V}}{Dt} = -\nabla(p + \gamma z) + \mu \nabla^2 \vec{V}$$

where $\frac{D\phi}{Dt}$ is the material derivative of function ϕ and γ is the specific weight which is the product of density and gravitational accelaration.

All the variables are nondimensionalized in terms of *ρ,* U and L, where U is some reference velocity and L is some reference length. The various dimensionless parameters can be written as

$$\vec{V}^* = \frac{\vec{V}}{U}, \qquad \vec{t}^* = \frac{tU}{L}, \qquad \vec{x}^* = \frac{\vec{x}}{L}, \qquad p^* = \frac{p + \rho g z}{\rho U^2}$$

the remaining parameters can be put into a nondimensional form by substituting $\vec{V}^* U = \vec{V}$, to obtain

$$\frac{\partial}{\partial t} = \frac{\partial}{\partial t^*}\frac{\partial t^*}{\partial t} = \frac{U}{L}\frac{\partial}{\partial t^*} \ ,$$

$$\nabla = \frac{\partial}{\partial x}\hat{\imath} + \frac{\partial}{\partial y}\hat{\jmath} + \frac{\partial}{\partial z}\hat{k} = \frac{\partial}{\partial x^*}\frac{\partial x^*}{\partial x}\hat{\imath} + \frac{\partial}{\partial y^*}\frac{\partial y^*}{\partial y}\hat{\jmath} + \frac{\partial}{\partial z^*}\frac{\partial z^*}{\partial z}\hat{k} = \frac{1}{L}\nabla^* \ ,$$

$$\frac{\partial u}{\partial x} = \frac{1}{L}\frac{\partial}{x^*}(Uu^*) = \frac{U}{L}\frac{\partial u^*}{\partial x^*},$$

Substituting the appropriate variables into the momentum equation yields the following nondimensionalized momentum equation

$$\frac{D\vec{V}^*}{Dt} = -\nabla^* p^* + \frac{\mu}{\rho V L}\nabla^{*2}\,\vec{V}^*$$

Where $\frac{\mu}{\rho V L}$ is the reciprocal of the Reynolds Number, which can be written as

$$Re = \frac{\rho V L}{\mu}, \text{ Reynolds Number}$$

The Reynolds number is a dimensionless number that represents the ratio of inertia forces to viscous forces. Similar nondimensionalization of the continuity equation leads to the Froude number, which represents the ratio of inertia forces to gravity force and can be written as

$$Fr = \frac{V}{\sqrt{gL}}, \text{ Froude Number}$$

Other nondimensional number used in flow computation include Mach Number, which is the ratio of inertia force and compressibility force, and the Pressure Coefficient, which is ratio of pressure force to inertia force. Equations for the two numbers can be written as such

$$Ma = \frac{V}{a}, \text{ Mach Number where a is the speed of sound in liquid}$$

$$C_p = \frac{\Delta p}{\rho V^2}, \text{ Coefficient of Pressure}$$

Flow conditions for model test and prototype test are completely similar if all relevant dimensionless parameters have the same values for both model and prototype. This similarity in all dimensionless parameters is sometimes difficult to achieve. Therefore it is often necessary to achieve

similarity in those dimensionless numbers that are most important to your case study. In this case the Reynolds number will have greater importance and will be given greater consideration, where as the Froude number and Mach number will be accommodated as best as possible.

Chapter 6: Cost Analysis

Table 5: Cost Breakdown

Part Number	Part Name	Quantity	Price
1	Wing-Body Configuration	1	70
2	Optimal Winglet #1	1	20.3
3	Optimal Winglet #2	1	20.3
4	Optimal Winglet #3	1	20.3
5	West System Marine Epoxy	2 qt.	81.29
6	Slow Hardener	1 pt.	42.77
7	Embry-Riddle Wind Tunnel Testing	5 hrs.	875
		Total	**1129.96**

Conclusions

Moderating the cost of keeping an aircraft in the air, getting revenue, is a constant challenge. With jet fuel prices skyrocketing, a more fuel-efficient design is always in demand. Wing design and particularly winglet and winglet configurations are an important feature that is constantly evolving. They help reduce induce drag and increase lift, helping improve the overall efficiency of the aircraft. What started off as a simple end plate design has now evolved into a more elegant and efficient blended winglet technology. To find the best optimum design, concepts from over the globe have to be investigated. As shown before, the wingtip fence is used by the French manufacturer, Airbus, while the Blended and Scimitar Winglets are used by Boeing. This shows the needs for global learning, and it through a combination of these two designs that a more efficient solution is obtained.

It is possible to further optimize these blended winglets, with an addition of a cost effective ventral strake. This eliminates the need to design and construct an entirely new winglet, thus reducing computational and manufacturing cost. The Wingtip fence has also shown promising results in making the wing more efficient. It is beneficial to investigate and compare the two winglets to see the benefits of each. The goal for this project is to investigate the effectiveness of the multi-winglets over Wingtip Fence and Blended winglets and to further improve the existing blended winglet design by 2% with the addition of the ventral strake.

References

[1]. Pandey, Kumar, Surana, Deka, "CFD Analyss of Airbus A380 Isolated Wings During Take-Off, Cruising and Landing and Comparison with Low Reynolds Number, High Lift S1223 Airfoil," International Review of Aerospace Engineering (I.RE.AS.E), Vol. 5, No.3, 2012.

[2]. Takenaka, Hatanaka, Kakahashi, "Multi-Disciplinary Design Exploration for Winglet," Proceedings of the 26th International Congress of Aeronautical Sciences (ICAS), 2008.

[3]. Maughmer, Kunz, "Sailplane Winglet Design," Presented at the XXV OSTIV Congress, Saint Auban, France.

[4]. Azlin, Taib, Kasolang, Muhammad, "CFD Analysis of Winglets at Low Subsonic Flow," Proceedings of the World Congress on Engineering (WCE), Vol I, London, U.K. July 6- 8, 2011.

[5]. Maughmer, "The Design of Winglets For Low-Speed Aircraft,"

[6]. Jacob, "Corotating Wake Vortex Formation, Merger & Modification," Proceedings of the DFD Meeting of The American Physical Society, November 21, 2005.

[7]. Dimitri, "Numerical Inverstigation of Blended Winglet Effects on Wing Performances," Fluid and Combustion Engineering, FACE10, Spring 2008.

[8]. Rajendran, "Design of Parametric Winglets and Wing tip devices – A Conceptual Design Approach," Linköping University Electronic Press, Linköping, Sweden, 2013

[9]. Ning, Kroo, "Tip Extensions, Winglets, and C-Wings: Conceptual Design and Optimization," AIAA,

[10]. Belkhiri, Boulahia, Belghar, “Numerical Simulation of Aerodynamics Performance for Winglet in the Low Speed compressible flow,” Revue des Energies Renouvelables CISM ’08 Oum El Bouaghi, 2008.

[11] “To Reality: Winglets.” Langevin,G.S. and Overbey, P. NASA Langley Research Center, October 17, 2003

[12] “Fluent 6.2 User’s Guide”, November 2013.

[13] Drela, M., “XFOIL Documentation,” User's Guide, Mark Drela, Cambridge, MA, c. 1989.

[14] Dennis, Dulikravich, Han, “Optimization of Turbomachinery Airfoil with a Genetic/Sequential-Quadratic-Programming Algorithm,” Journal of Propulsion and Power, Vol. 17, No. 5, 2001.

[15] Heintz,”Airfoils”, EAA Light Plane World magazine, 1987.

[16] Cella,” Assessment of Optimization Algorithms for Winglet Design,”*EnginSoft Newsletter Year 7 n.1*

[17] "The Shapes of the Future." *Aviation Partners Inc.* N.p., n.d. Web. 24 Nov. 2013.

[18] "Wingtip Device." *Wikipedia*. Wikimedia Foundation, 23 Nov. 2013. Web. 24 Nov. 2013.

[19] Meinhard Schobeiri, “Fluid Mechanics for Engineers: A Graduate Textbook,” 2010

[20] Menter, “Turbulence Modeling for Engineering Flows”, A Technical Paper from ANSYS, inc.

[21] LeVeque, Randall (2002), Finite Volume Methods for Hyperbolic Problems, Cambridge University Press.

[22] Toro, E. F. (1999), Riemann Solvers and Numerical Methods for Fluid Dynamics, Springer-Verlag.

[23] Stren,F., “Mechanics of Fluids and Transport Processes”, 2013, Ch 7.